Supplementary Information

Understanding surface chemical processes in perovskite oxide electrodes

Zijie Sha, Zonghao Shen, Eleonora Calì, John A. Kilner, and Stephen J. Skinner

Dept. of Materials, Exhibition Road, Imperial College London, London, SW7 2AZ, UK.

zonghao.shen12@imperial.ac.uk

s.skinner@imperial.ac.uk

SECTION S-1:

For the quantitative analysis on the LEIS spectra, the first step is to subtract the background component. The background in LEIS spectra is produced through a combination of the secondary ions sputtered by the projectiles and the projectile ions scattered by the atoms below the surface (also referred to as the 'in-depth signal)[1]. In a typical LEIS spectrum, towards lower energies there is an exponential increase in the signal which obscures the peaks in the region and affects further quantitative analysis due to the sputtered secondary ions. The most common sputtered background ion is from the surface absorbed hydrogen which is ionised during a sputtering event[2]. Other contaminants with high positive ionisation probabilities (e.g. hydrocarbons, sodium) in the top surface layers also contributes to the background signals, and this effect is particularly prominent during the first analysis cycles of the depth profile. The exponential background signal can be straightforwardly subtracted using the SurfaceLab6 software from IONTOF or other data processing software, e.g. OriginLab, Matlab etc. In this work, the background was mainly subtracted with the SurfaceLab6 and after the exponential subtraction, the residual background for Cr and Fe was already negligible, while for La and Sr the 'in-depth' background requires further subtraction. This 'in-depth' background signal is due to noble gas ions that have entered the sample, been neutralised, been losing energy during stoppage events by electrons and nuclei, been backscatted and been reionised when the noble gas atoms leave the solid sample, especially for oxides[2,3]. This will result in a long and relatively flat tail towards the lower energy of the peak. Albeit the shapes and lengths of the tails provide additionally information on in-depth distribution of elements and physical depth in the sample, the 'in-depth' background is undesired for surface composition analysis and SurfaceLab6 software can also subtract the remaining 'in-depth' background signal using modified complementary error functions. An example of background subtracted $^{20}Ne^{+}$ (5 keV) LEIS spectrum is illustrated in Figure S1.

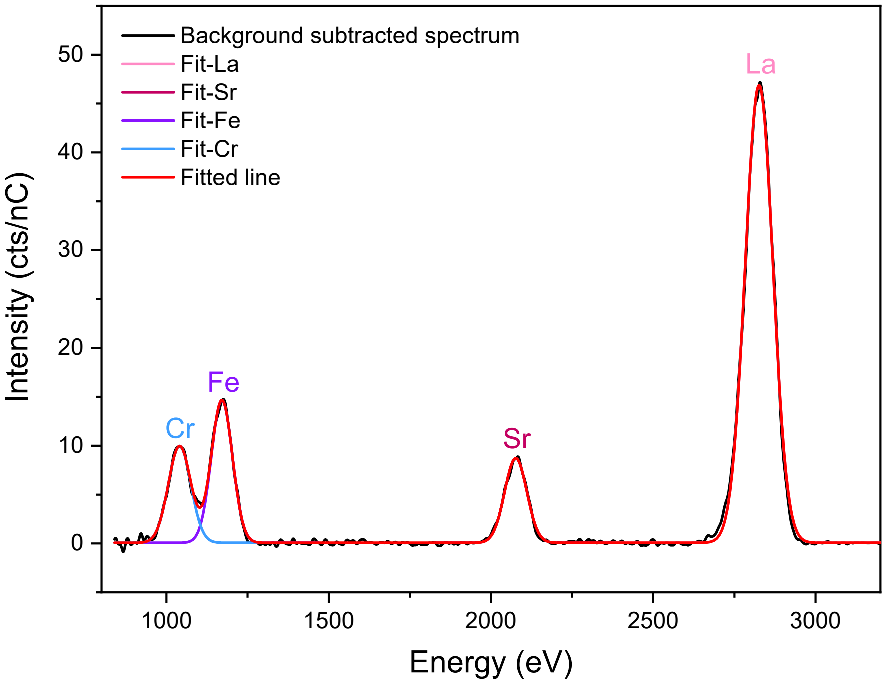

Figure S1. An example of the fitted scattering peaks in a typical $^{20}Ne^{+}$ (5 keV) LEIS spectrum obtained from LSCrF8255 after subtracting the background.

In Figure S1, the scattering peaks are fitted by a Gaussian distribution, with correction of isotopic distribution for each element and fixed peak width and position. The peak width and position were determined by fitting the overall spectrum on a per-sample basis. The peak areas can thus be obtained.

The quantification of the cation fractional coverage on a surface was performed based on an assumption that the plateau region after sufficient sputter fluence corresponds to the nominal bulk cation stoichiometry, which is also confirmed by XPS analysis. The preferential sputtering of the cation species[1] is considered and referenced to the results of the measurement carried out on the as-polished sample's cross-section. The preferential sputtering parameter for the A-site cation species, α, and B-site cation species, β, are defined in Equation S1:

$$\alpha = \frac{I_{La}/C_{La}}{I_{Sr}/C_{Sr}},\ \beta = \frac{I_{Fe}/C_{Fe}}{I_{Cr}/C_{Cr}} \qquad \text{Equation S1}$$

where I denotes the integral of the obtained scattering peak of the corresponding element in the plateau region after sputtering, and C denotes the nominal bulk concentration for the corresponding element. The α and β values obtained from the cross-section are 1.66 and 1.42 respectively and they should remain constant for all LSCrF8255 samples during the whole depth profiling process. Thus the surface concentration for A-site and B-site elements can be further obtained. The LEIS depth profiles of the ratio of total Sr content $[Sr]_{total}$ over the total La content $[La]_{total}$ ($[Sr]_{total} : [La]_{total}$), total Cr content $[Cr]_{total}$ over the total Fe content $[Fe]_{total}$ ($[Cr]_{total} : [Fe]_{total}$), and total A-site cation content over total B-site cation content ($[Sr]+[La]$) : ($[Cr]+[Fe]$) as a function of Ar^{+} fluence obtained from the cross-section of the as-polished sample are illustrated in Figure S2.

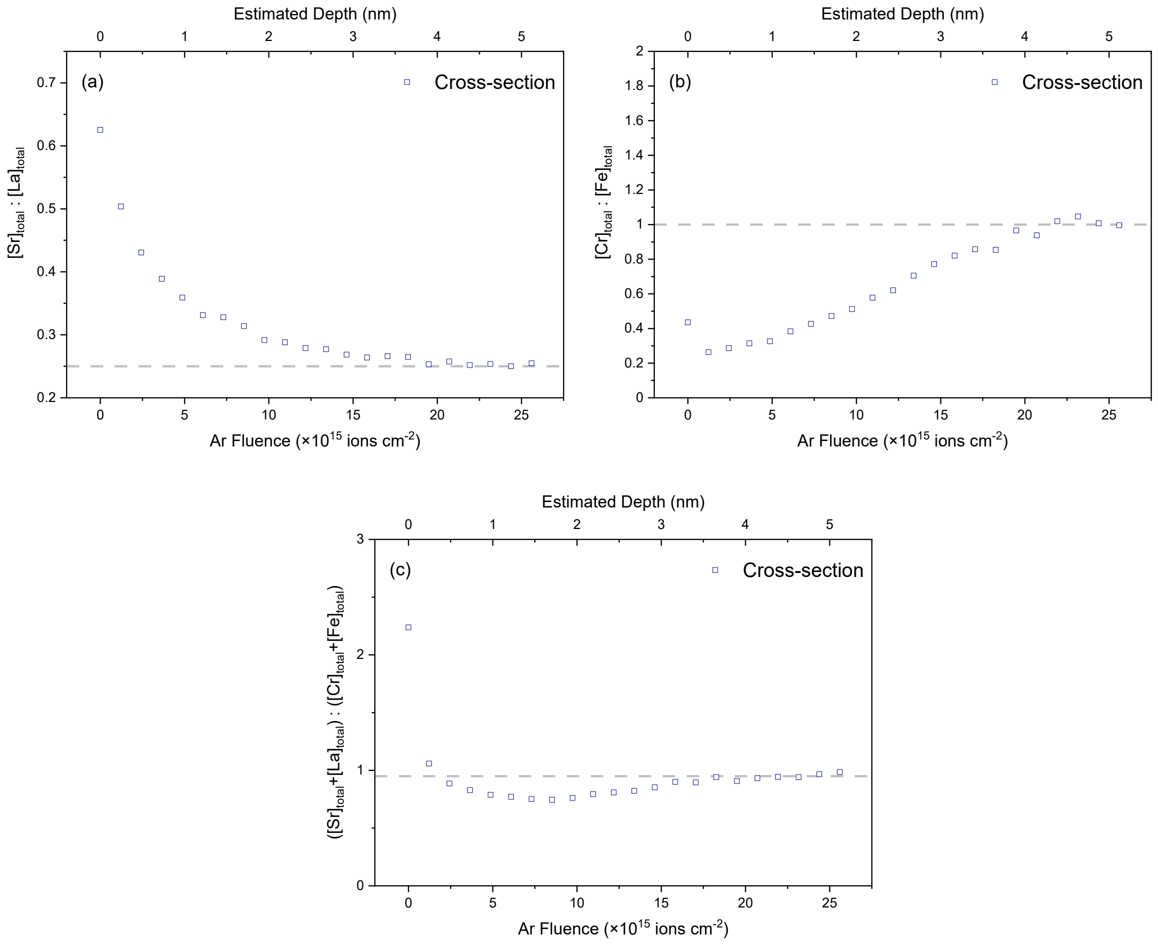

Figure S2. (a – c) LEIS depth profiles showing atomic ratio of (a) $[La]_{total} : [Sr]_{total}$; (b) $[Cr]_{total} : [Fe]_{total}$, and (c) ([Sr]+[La]) : ([Cr]+[Fe]) collected from the cross-section of an as-polished LSCrF8255 sample. The dashed line indicates the bulk stoichiometry.

The depth estimations on the LEIS depth profiles were based upon the instrumental value of 2 Å/10 × 10^{15} ions cm^{-2} tested on a Si wafer, which is close to the approximate value of 2.6 Å/10 × 10^{15} ions cm^{-2} estimated by Druce et al.[4] on $La_{0.6}Sr_{0.4}Co_{0.2}Fe_{0.8}O_{3-\delta}$, a material with similar density, crystal structure and lattice parameters to LSCrF8255. The sputter rate was assumed to be constant throughout the whole depth profile. However, factors such as grain orientation, preferential sputtering and chemical compositional changes will have an effect on the sputter rate which requires further studies.

SECTION S-2:

Table S1. The atomic ratio of $[\mathrm{Sr}]_{\mathrm{surface}} : [\mathrm{Sr}]_{\mathrm{bulk}}$ and $[\mathrm{Sr}]_{\mathrm{total}} : [\mathrm{La}]_{\mathrm{total}}$ measured from the LSCrF8255 samples annealed in dry oxygen, wet oxygen, and water vapour conditions at 600, 700, 800, and 900 °C for 27 hours through XPS (≈ 10 nm probe depth) and ARXPS (< 1 nm probe depth). The data measured in wet oxygen was taken from[5], the data measured in water vapour was taken from[6].

T (°C)	**Dry oxygen annealed**				**Wet oxygen annealed**[6]				**Water vapour annealed**			
	$[\mathrm{Sr}]_{\mathrm{surface}} : [\mathrm{Sr}]_{\mathrm{bulk}}$		$[\mathrm{Sr}]_{\mathrm{total}} : [\mathrm{La}]_{\mathrm{total}}$		$[\mathrm{Sr}]_{\mathrm{surface}} : [\mathrm{Sr}]_{\mathrm{bulk}}$		$[\mathrm{Sr}]_{\mathrm{total}} : [\mathrm{La}]_{\mathrm{total}}$		$[\mathrm{Sr}]_{\mathrm{surface}} : [\mathrm{Sr}]_{\mathrm{bulk}}$		$[\mathrm{Sr}]_{\mathrm{total}} : [\mathrm{La}]_{\mathrm{total}}$	
	XPS	AR-XPS	XPS	AR-XPS	XPS	AR-XPS	XPS	AR-XPS	XPS	AR-XPS	XPS	AR-XPS
600	34 : 66	59 : 41	11 : 89	13 : 87	31 : 69	44 : 55	17 : 83	18 : 82	25 : 75	51 : 49	17 : 83	19 : 81
700	42 : 58	59 : 41	11 : 89	12 : 88	44 : 56	67 : 33	18 : 82	20 : 80	36 : 64	70 : 30	18 : 82	20 : 80
800	63 : 37	78 : 22	18 : 82	23 : 77	53 : 47	80 : 20	20 : 80	21 : 79	52 : 48	81 : 19	21 : 79	14 : 76
900	67 : 33	81 : 19	28 : 72	41 : 59	66 : 34	83 : 17	18 : 82	21 : 79	93 : 7	97 : 3	24 : 76	28 : 72

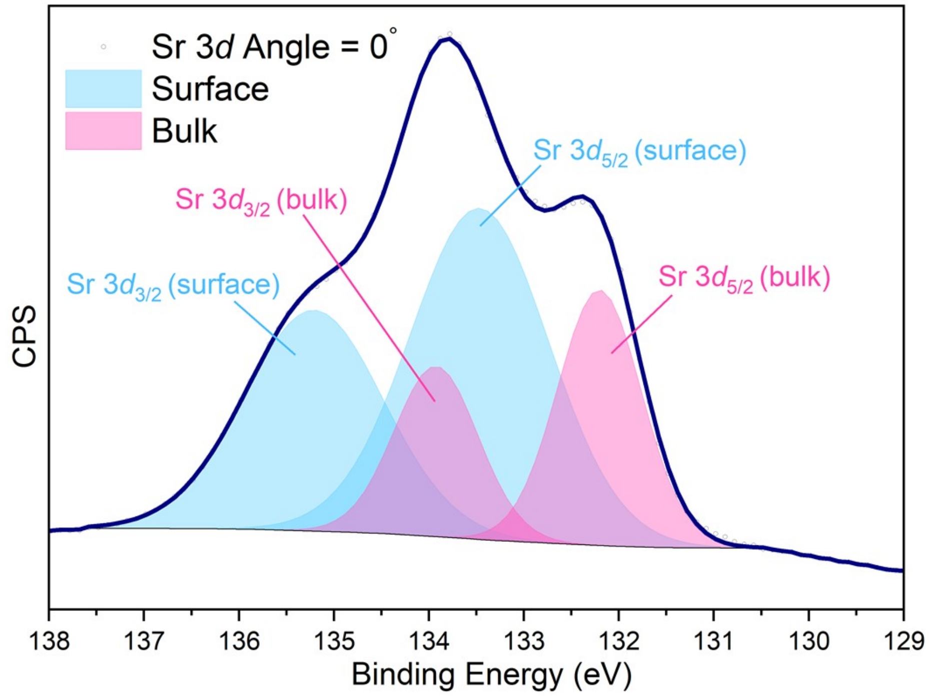

Figure S3. An example of fitted Sr 3*d* XPS spectrum collected from the LSCrF8255 sample annealed in dry oxygen at 900 °C.

Table S2. The atomic ratio of $[\mathrm{Sr}]_{\mathrm{surface}}:[\mathrm{Sr}]_{\mathrm{bulk}}$ and $[\mathrm{Sr}]_{\mathrm{total}}:[\mathrm{La}]_{\mathrm{total}}$ obtained from an as-polished sample.

$[\mathrm{Sr}]_{\mathrm{surface}}:[\mathrm{Sr}]_{\mathrm{bulk}}$		**$[\mathrm{Sr}]_{\mathrm{total}}:[\mathrm{La}]_{\mathrm{total}}$**	
XPS	AR-XPS	XPS	AR-XPS
11 : 89	13 : 87	17 : 83	17 : 83

Table S3. The atomic ratio of $[\mathrm{Cr}]_{\mathrm{total}}:[\mathrm{Fe}]_{\mathrm{total}}$ obtained from an as-polished sample, and the samples annealed in dry oxygen, wet oxygen, and water vapour at 900 °C for 27 hours through XPS (≈ 10 nm probe depth) and ARXPS (< 1 nm probe depth).

Sample	**$[\mathrm{Cr}]_{\mathrm{total}}:[\mathrm{Fe}]_{\mathrm{total}}$**	
	XPS	ARXPS
As-polished	48:52	49:51
Dry oxygen 900 °C	48:52	52:48
Wet oxygen 900 °C	50:50	50:50
Water vapour 900 °C	52:48	50:50

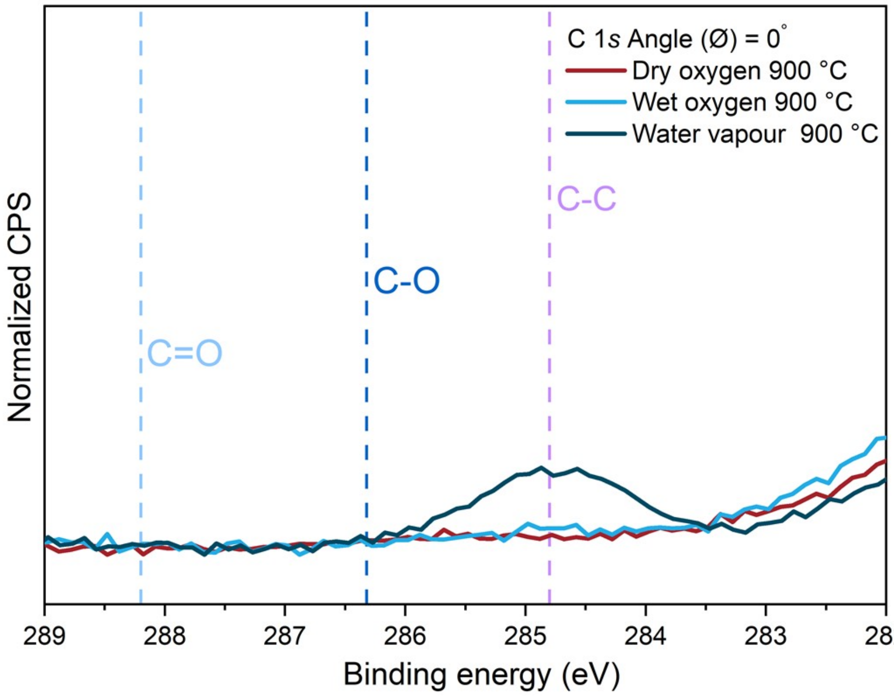

Figure S4. The C 1*s* spectra collected from LSCrF8255 samples annealed in dry oxygen, wet oxygen, and water vapour atmospheres at 900 °C for 27 hours.

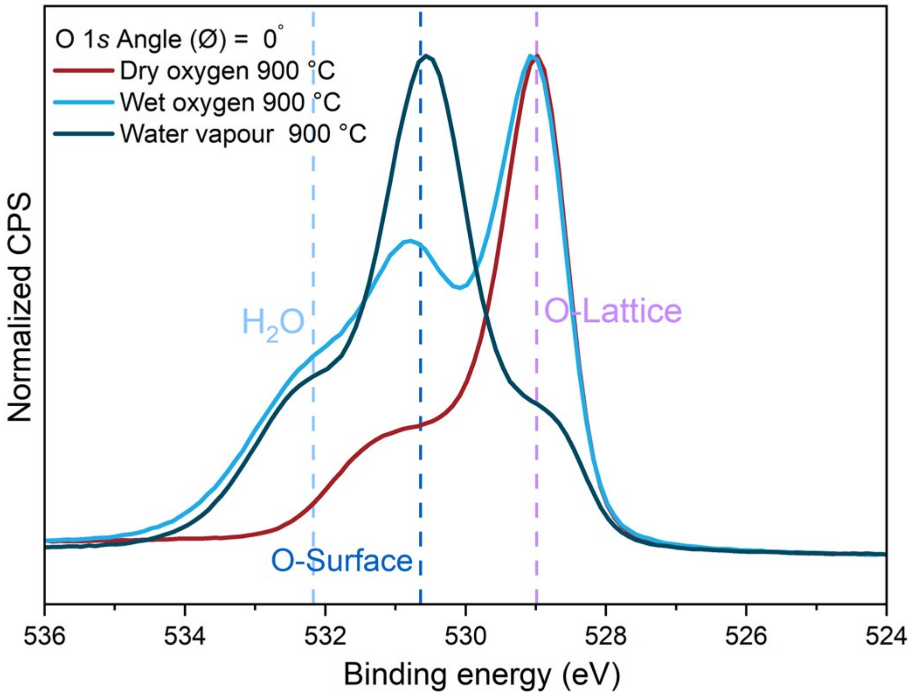

Figure S5. The O 1*s* spectra collected from LSCrF8255 samples annealed in dry oxygen, wet oxygen, and water vapour atmospheres at 900 °C for 27 hours.

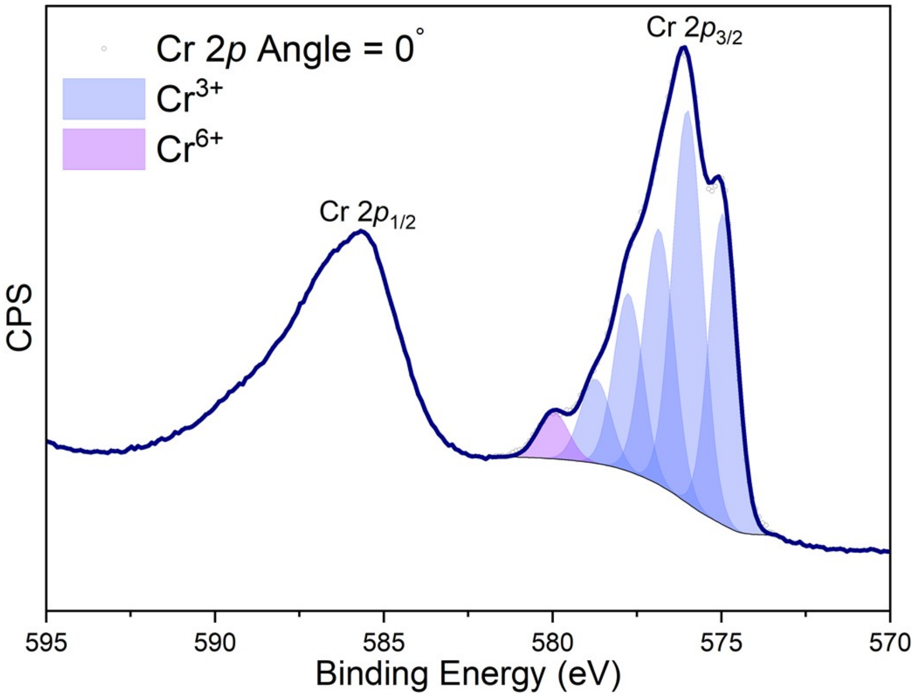

Figure S6. An example of fitted Cr 2*p* XPS spectrum collected from the LSCrF8255 sample annealed in dry oxygen at 900 °C.

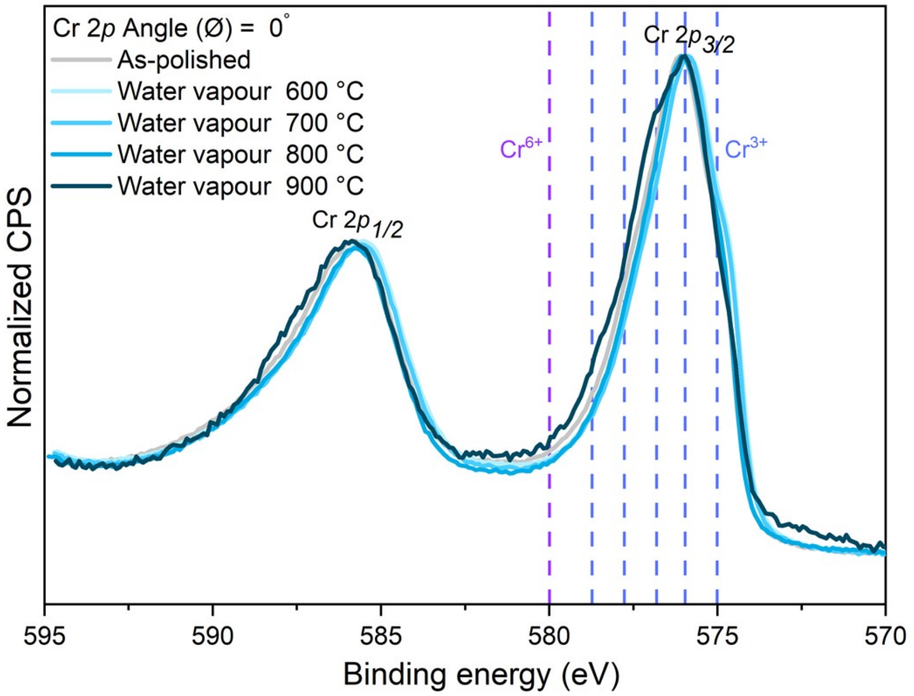

Figure S7. The Cr 2p spectra of the as-polished sample and samples annealed in water vapour at 600, 700, 800, and 900 °C.

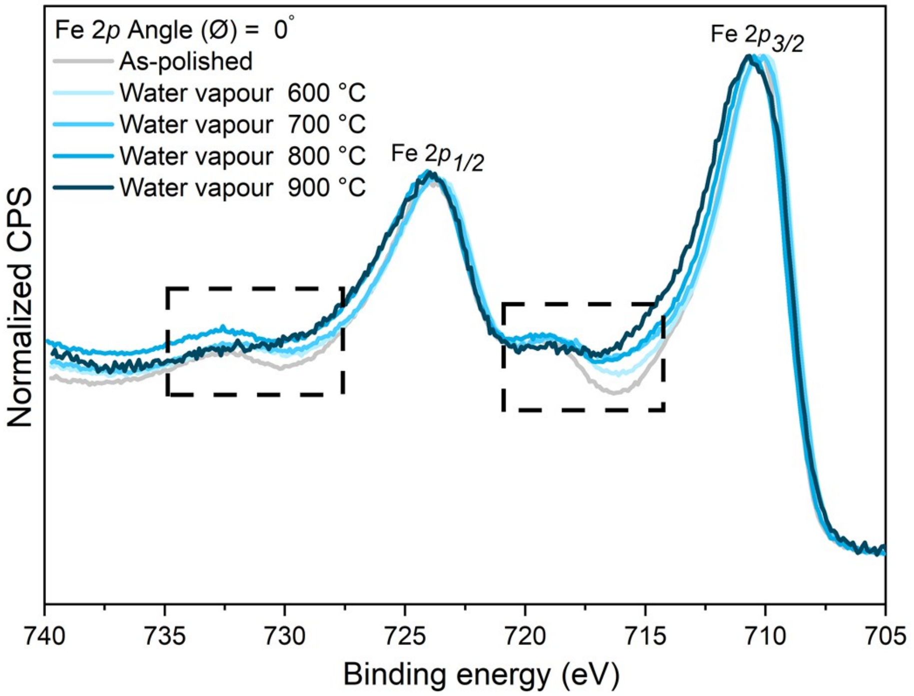

Figure S8. The Fe 2*p* spectra of the as-polished sample and samples annealed in water vapour at 600, 700, 800, and 900 °C.

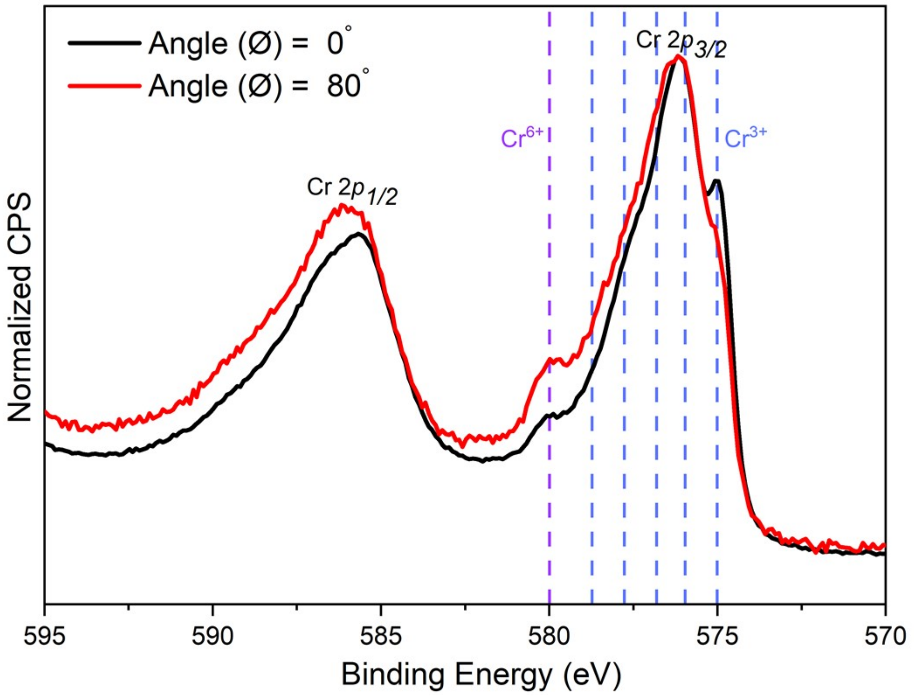

Figure S9. The XPS (black) and ARXPS (red) spectra of Cr 2*p* collected from the annealed LSCrF8255 sample in dry oxygen at 900 °C for 27 hours.

Table S4. The atomic ratios of [Cr^{6+}]:[Cr^{3+}] and $[Cr]_{total}$:$[Fe]_{total}$, obtained from the LSCrF8255 sample annealed in dry oxygen at 900 °C for 27 hours through XPS (≈ 10 nm probe depth) and ARXPS (< 1 nm probe depth).

[Cr^{6+}] : [Cr^{3+}]		**$[Cr]_{total}$: $[Fe]_{total}$**	
XPS	ARXPS	XPS	ARXPS
4 : 96	7 : 93	48 : 52	52 : 48

Table S5. The atomic ratio of $[Si]_{total}$: $[La]_{total}$ collected from the LSCrF8255 samples annealed in wet oxygen and water vapour at 900 °C for 27 hours through XPS (≈ 10 nm probe depth) and ARXPS (< 1 nm probe depth).

T (°C)	**Wet oxygen annealed sample $[Si]_{total}$: $[La]_{total}$**		**Water vapour annealed sample $[Si]_{total}$: $[La]_{total}$**	
	XPS	ARXPS	XPS	ARXPS
900	39 : 61	50 : 50	50 : 50	63 : 37

SECTION S-3:

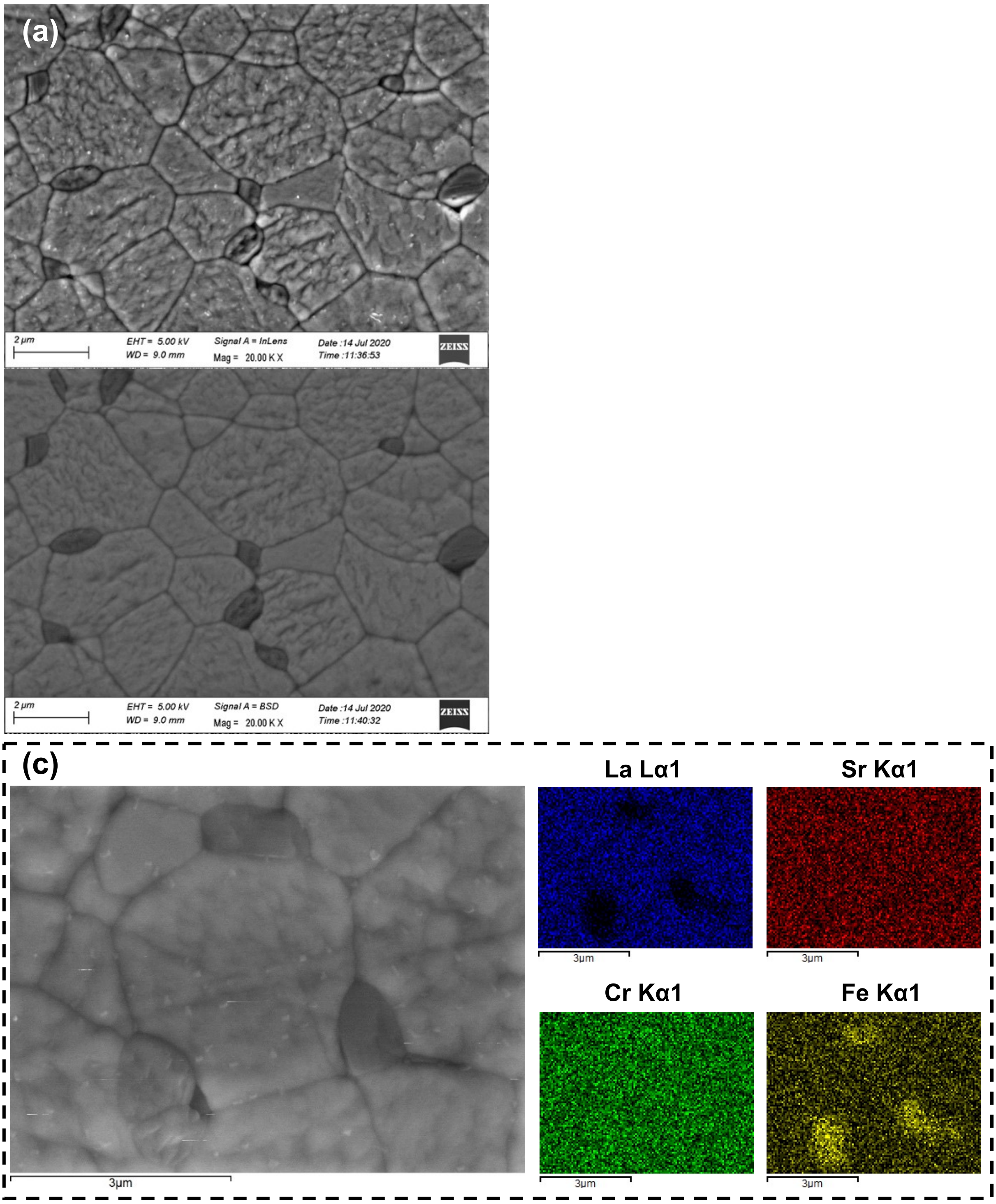

Figure S10. (a – c) The (a) SE image, (b) BSE image, and (c) SEM-EDX map of the sample annealed in dry oxygen at 900 °C for 27 hours.

SECTION S-4:

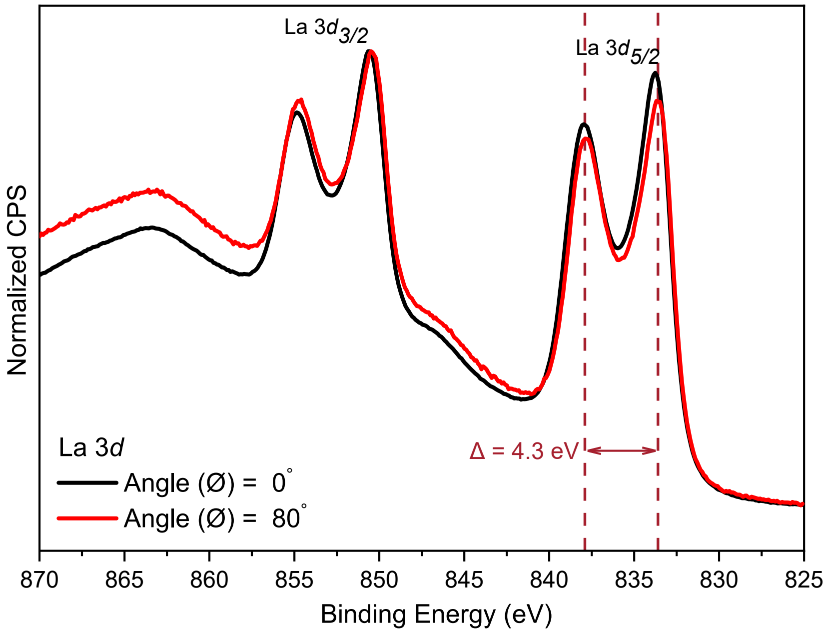

Figure S11. The XPS (black) and ARXPS (red) spectra of La 3*d* collected from the annealed LSCrF8255 sample in dry oxygen at 700 °C.

Table S6. The atomic ratio of $[Cr^{6+}]:[Cr^{3+}]$ and $[Cr]_{total}:[Fe]_{total}$ obtained from the LSCrF8255 samples annealed in dry oxygen (pO_2 = 200 mbar) at 600 and 700 °C for 27 hours through XPS (≈ 10 nm probe depth) and ARXPS (< 1 nm probe depth).

T (°C)	**$[Cr^{6+}]:[Cr^{3+}]$**		**$[Cr]_{total}:[Fe]_{total}$**	
	XPS	ARXPS	XPS	ARXPS
600	5 : 95	9 : 91	51 : 49	56 : 44
700	6 : 94	10 : 90	50 : 50	57 : 43

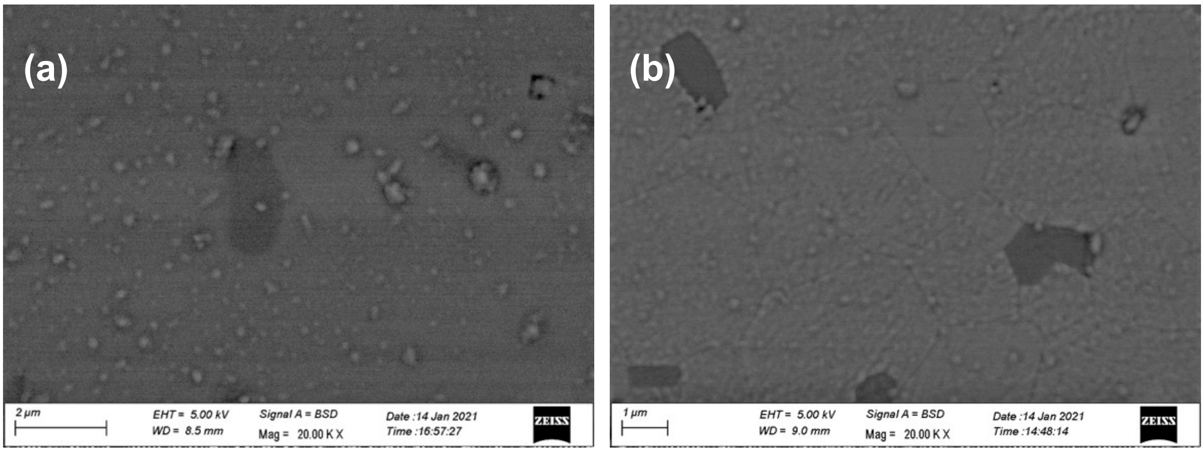

Figure S12. (a – b) The SEM BSE images of the LSCrF8255 samples annealed at (a) 600 °C; (b) 700 °C for 27 hours.

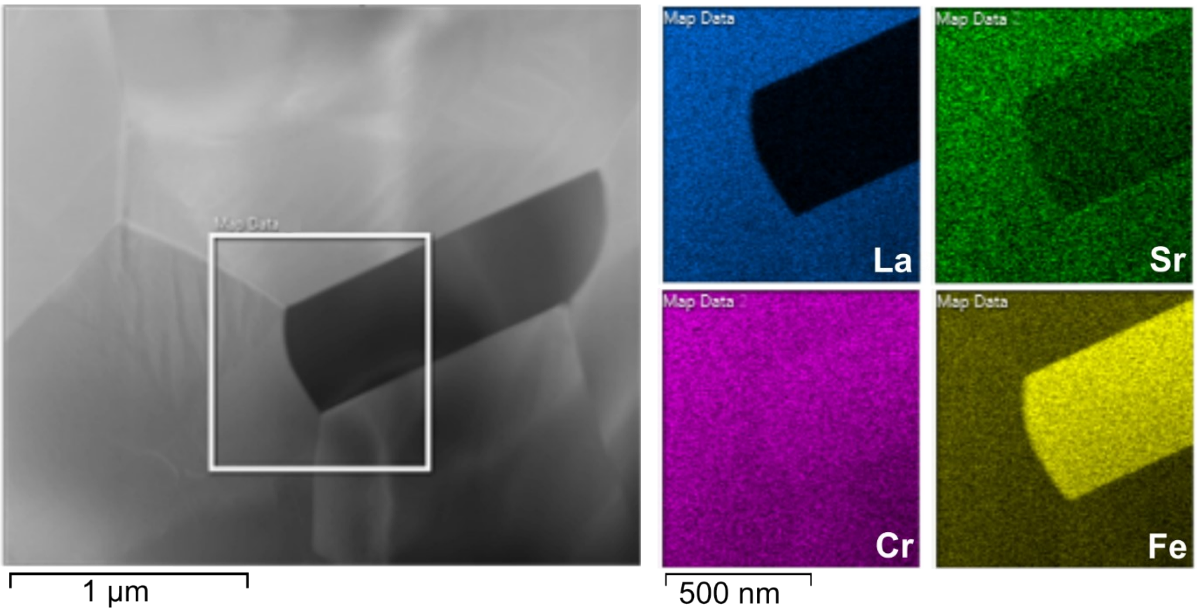

Figure S13. STEM-EDX map collected on the sample annealed in dry oxygen at 600 °C.

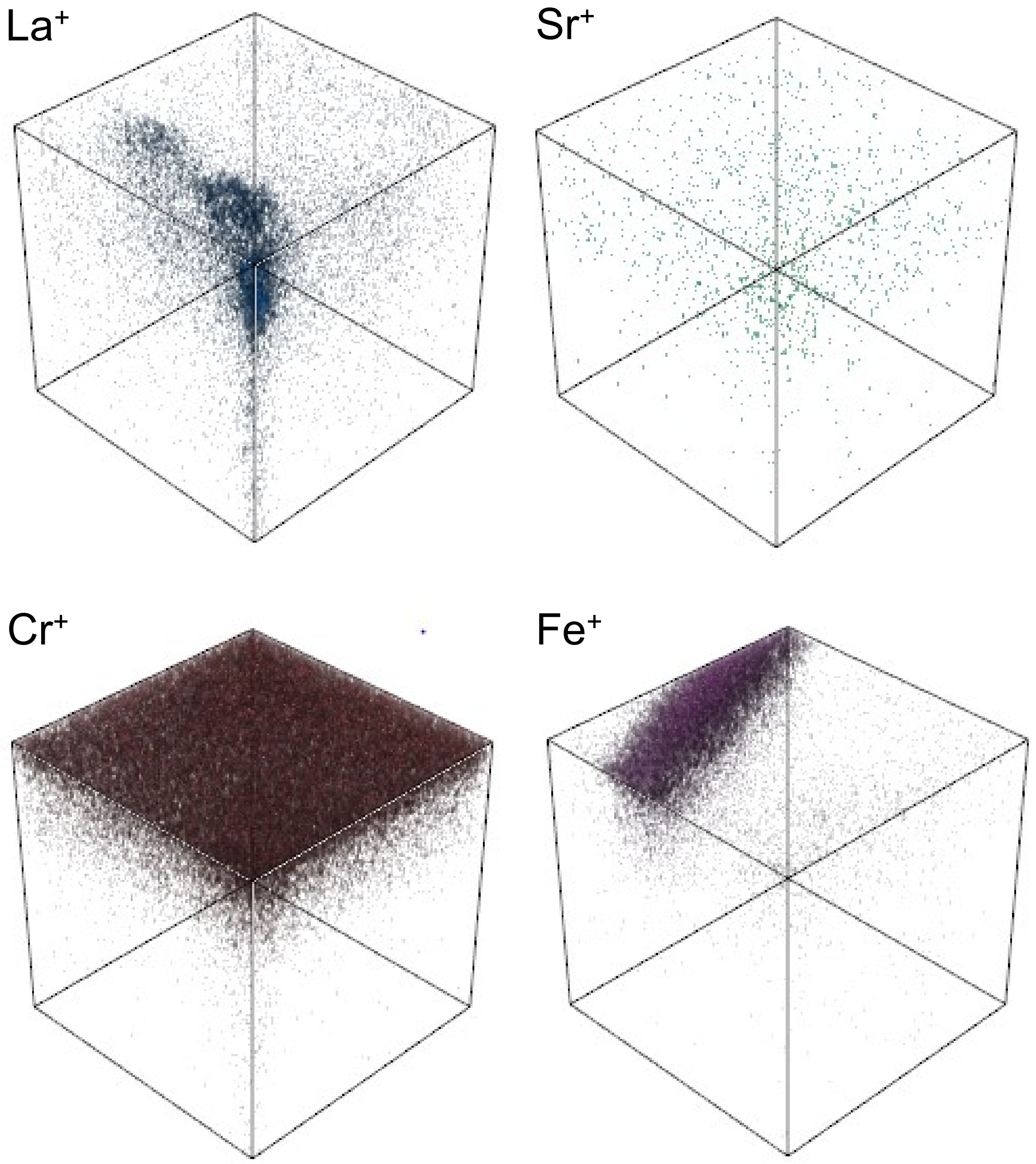

Figure S14. 3D reconstruction of the La$^+$, Sr$^+$, Cr$^+$, and Fe$^+$ signals detected on the Si wafer annealed alongside a LSCrF8255 at 600 °C in dry oxygen for 11 days.

Table S7. The normalized intensities of the La$^+$, Sr$^+$, Cr$^+$, and Fe$^+$ signals detected on the Si wafer annealed alongside a LSCrF8255 at 600 °C in dry oxygen for 11 days. The intensities were estimated with the relative sensitivity factors (RSF) of elements on Si wafer under an oxygen sputtering beam[7] and normalized with ^{56}Fe.

La$^+$	**Sr$^+$**	**Cr$^+$**	**Fe$^+$**
3.6	6.5	18.7	1.0

Table S8. The atomic ratio of $[Sr]_{surface}:[Sr]_{bulk}$ and $[La]_{total}:[Sr]_{total}$ of LSCrF8255 annealed in dry oxygen at 600 °C as a function of annealing time through XPS (≈ 10 nm probe depth) and ARXPS (< 1 nm probe depth).

T (°C)	**Exchange duration**	$[Sr]_{surface}:[Sr]_{bulk}$		$[La]_{total}:[Sr]_{total}$	
		XPS	ARXPS	XPS	ARXPS
600	27 hours	34:66	59:41	89:11	87:13
600	8 days	32:68	56:44	90:10	91:9

REFERENCES

1. Niania, M., Sharpe, M., Webb, R. & Kilner, J. A. The surface of complex oxides; ion beam based analysis of energy materials. *Nuclear Instruments and Methods in Physics Research, Section B: Beam Interactions with Materials and Atoms* **480**, 27–32 (2020).

2. Cushman, C. v. *et al.* Low energy ion scattering (LEIS). A practical introduction to its theory, instrumentation, and applications. *Analytical Methods* vol. 8 3419–3439 (2016).

3. Brongersma, H. H., Draxler, M., de Ridder, M. & Bauer, P. Surface composition analysis by low-energy ion scattering. *Surface Science Reports* **62**, 63–109 (2007).

4. Druce, J. *et al.* Surface termination and subsurface restructuring of perovskite-based solid oxide electrode materials. *Energy and Environmental Science* **7**, 3593–3599 (2014).

5. Sha, Z., Cali, E., Kerherve, G. & Skinner, S. J. Oxygen diffusion behaviour of A-site deficient $(La_{0.8}Sr_{0.2})_{0.95}Cr_{0.5}Fe_{0.5}O_{3-\delta}$ perovskites in humid conditions. *Journal of Materials Chemistry A* **8**, 21273–21288 (2020).

6. Sha, Z. *et al.* Significantly Enhanced Oxygen Transport Properties in Mixed Conducting Perovskite Oxides under Humid Reducing Environments. *Chemistry of Materials* **33**, 8469–8476 (2021).

7. Wilson, R. G., Stevie, F. A. & Magee, C. W. Secondary ion mass spectrometry: a practical handbook for depth profiling and bulk impurity analysis. *Anal Chim Acta* **242**, 301 (1991).